Tide-Induced Variations in Surface Temperature and Water-Table Depth in the Intertidal Zone of a Sandy Beach

Author(s): Ling Li, Diane P. Horn and Andrew J. Baird

Source: *Journal of Coastal Research*, Nov., 2006, Vol. 22, No. 6 (Nov., 2006), pp. 1370-1381

Published by: Coastal Education & Research Foundation, Inc.

Stable URL: https://www.jstor.org/stable/30138403

JSTOR is a not-for-profit service that helps scholars, researchers, and students discover, use, and build upon a wide range of content in a trusted digital archive. We use information technology and tools to increase productivity and facilitate new forms of scholarship. For more information about JSTOR, please contact support@jstor.org.

Your use of the JSTOR archive indicates your acceptance of the Terms & Conditions of Use, available at https://about.jstor.org/terms

is collaborating with JSTOR to digitize, preserve and extend access to *Journal of Coastal Research*

This content downloaded from 152.15.113.8 on Thu, 14 Oct 2021 17:10:39 UTC
All use subject to https://about.jstor.org/terms

Journal of Coastal Research	22	6	1370–1381	West Palm Beach, Florida	November 2006

Tide-Induced Variations in Surface Temperature and Water-Table Depth in the Intertidal Zone of a Sandy Beach

Ling Li[†‡], Diane P. Horn[§], and Andrew J. Baird[††]

[†]Environmental Engineering Division, School of Engineering, The University of Queensland, St. Lucia QLD 4072, Australia
l.li@uq.edu.au

[‡]Centre for Eco-Environmental Modelling, Hohai University, Nanjing 210098, People's Republic of China
liling_cj@hhu.edu.cn

[§]School of Geography, Birkbeck College, University of London, London WC1E 7HX, United Kingdom

[††]Department of Geography, Sheffield University, Sheffield S10 2TN, United Kingdom

ABSTRACT

LI, L.; HORN, D.P., and BAIRD, A.J., 2006. Tide-induced variations in surface temperature and water-table depth in the intertidal zone of a sandy beach. *Journal of Coastal Research,* 22(6), 1370–1381. West Palm Beach (Florida), ISSN 0749-0208.

A field experiment was conducted to investigate the fluctuations of the beach water table and surface temperature in the intertidal zone of a sandy beach. Both the temperature and beach water-table height were found to be influenced largely by the tide and beach morphology. A two-dimensional groundwater flow model was developed to examine the relationship between temperature, water-table height (depth), and tide and beach morphology. As the tide fell, the beach face drainage was controlled by the local beach slopes and the spatial patterns of the water-table behavior corresponded to the features of the beach profile. The results showed links between the beach water-table depth and surface temperature during the falling tide period, indicating the role of solar radiation in heating the exposed beach surface. These results may have important implications for studies on beach ecosystems, *e.g.,* the interstitial fauna.

ADDITIONAL INDEX WORDS: *Infrared imagining, beach surface temperature, beach ecology, beach hydrology, beach processes modeling.*

INTRODUCTION

The intertidal zone of sand beaches is an important habitat for interstitial fauna, particularly the meiofauna (McIntyre, 1969). The meiofauna are animals ranging in size from approximately 0.1 to 1 mm (the size class of transition from micro- to macrofauna) that live within the sediments. Unlike the macrofauna, the meiofauna maintain constant contact with the sand particle surface and are totally dependent on the conditions within the beach, such as the moisture content and temperature (Pollock and Hummon, 1971; Campbell and Bate, 1998).

An essential feature of the intertidal zone is the periodically alternating submergence and exposure of the beach surface, which affects the conditions of the beach environment, *e.g.,* the water-table depth, moisture content, and temperature. In coarse sand beaches, the pore spaces in the sand are filled and drained as the tide rises and falls, leading to the water-table fluctuations and changes of the moisture content in the partially saturated zone (Pollock and Hummon, 1971). In fine sand beaches, the moisture content is much less responsive to the tides because of the presence of truncated capillary fringes, despite the water-table fluctuations (Atherton, Baird, and Wiggs, 2001). Thus the degree of the tidal influence on the intertidal-zone conditions and the interstitial fauna of sandy beaches depends on the sediment sizes.

DOI:10.2112/04-0202.1 received 18 April 2005; accepted in revision 25 August 2005.

Tide-induced water-table oscillations have been the subject of many recent studies (*e.g.,* Nielsen, 1990; Turner, 1993; Baird and Horn, 1996; Baird, Mason, and Horn, 1998; Raubenheimer, Guza, and Elgar, 1999; Li *et al.,* 2000). Much previous work has investigated the water-table behavior landward of the high tide mark. Few studies have looked exclusively at water tables in the intertidal zone. Exceptions include Atherton, Baird, and Wiggs (2001) who measured both the water table and moisture content in the intertidal zone of a mesotidal beach. Cartwright Nielsen, and Li (2004) conducted a series of laboratory experiments to study the characteristics of tidal water-table fluctuations in the intertidal zone, particularly the generation of the subharmonics.

In contrast to the numerous studies on beach groundwater dynamics, the temperature of the intertidal zone has been investigated less extensively. Pollock and Hummon (1971) reported detailed measurements of the temperature changes in a sandy beach subject to tidal oscillations. Large changes in temperature were observed over the tidal cycle in the late spring. Such changes mainly occurred in the uppermost 10 cm of the beach, with the maximum taking place at the sand surface. Pollock and Hummon (1971) attributed these temperature changes to the exposure of the beach surface to the atmosphere during the low tide. However, the link between the exposure and the temperature change is not clear. Questions remain as to what parameters control the temperature changes and what role the tides play in the process of heat transfer within the intertidal zone.

This content downloaded from
152.15.113.8 on Thu, 14 Oct 2021 17:10:39 UTC
All use subject to https://about.jstor.org/terms

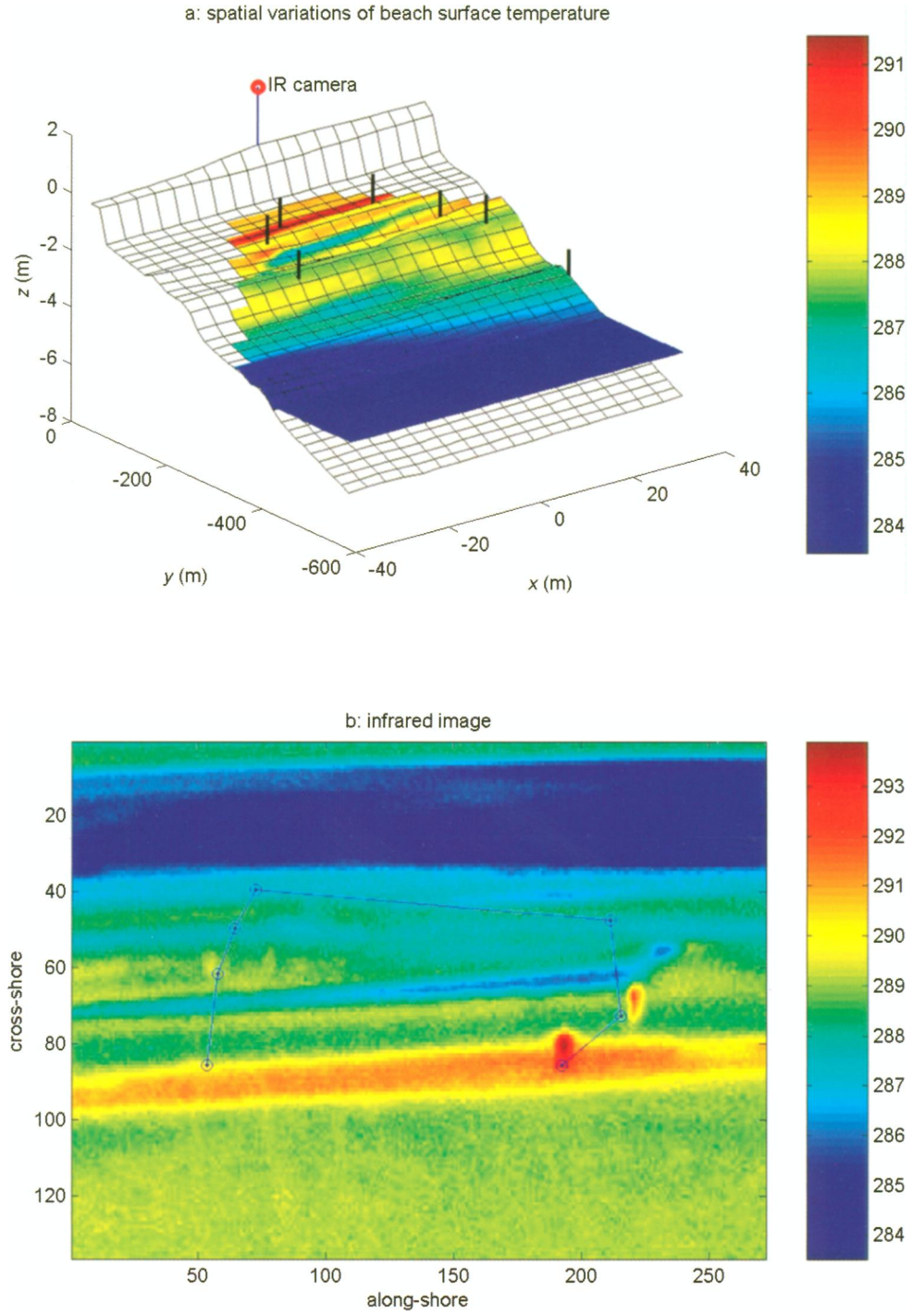

Figure 1. (a) Experiment area and setup. Vertical lines indicate the locations of the control points. (b) Infrared image.

The main purpose of this study was to investigate the mechanism and dynamics of beach surface heating due to exposure to solar radiation (sunlight) under the influence of tides. The surface temperature of a sand beach was monitored using a high performance infrared camera during a falling tide period. The data provided not only the temporal dynamics but also the spatial variations of the beach surface temperature. This allows examination of the relationship among the environmental parameters and conditions of the intertidal zone over a relatively large area. Clearly, the heat transfer process associated with the temperature changes is complex in a dynamic beach environment. Our modeling

This content downloaded from
152.15.113.8 on Thu, 14 Oct 2021 17:10:39 UTC
All use subject to https://about.jstor.org/terms

work has not attempted to simulate this process directly but rather has focused on the relationships among beach morphology, beach water-table fluctuations, and changes in beach temperature based on simple models. A secondary aim of this research was to investigate the potential of using infrared imaging techniques for monitoring beach surface conditions (*e.g.,* seepage face) based on temperature contrasts. Such techniques could be particularly useful at night when conventional methods (*e.g.,* visible-spectrum video) are not applicable or easily implemented.

FIELD EXPERIMENT AND RESULTS

The field experiment was conducted at Tentsmuir Beach in Scotland, a macrotidal, medium sand beach (d_{50} = 0.3 mm). The study area is as shown in Figure 1a. High-resolution survey of the beach surface temperature was conducted using a high performance infrared camera (AGEMA Infrared System AB). The camera was installed at a height of 9 m from ground level in the foreshore area, giving an effective surveying zone as shown by the color image of the temperature in Figure 1a. The temperature color image is superimposed on the beach surface in the exposed area and on the sea surface in the submerged area. The color bar indicates the surface temperature measured in degrees Kelvin (K). Seven control points were placed on the beach with the locations surveyed (vertical poles in Figure 1a). These control points were also captured by the infrared image as shown in Figure 1b. Mapping of the control points on the physical and image planes, based on the photometrical principle (STIMSON, 1974), gives the rule for determining the physical coordinates of the images, *i.e.,* converting Figure 1b to Figure 1a.

The experiment was conducted on July 31, 2001, during a larger field investigation lasting from July 15, 2001, to August 4, 2001. Over the entire period, the tides were measured using a seabed-mounted pressure transducer (Figure 2a). Five boreholes were installed along a cross-shore transect in the center of the area (Figure 2b). The water level fluctuations in these boreholes were monitored. The beach profiles over an area of 500 m (cross-shore distance) by 80 m (along distance) were surveyed on a daily basis. All these data were used to run and verify the model, which was developed to examine the fluctuations of the beach water table and surface temperature.

The raw tidal data, displayed by the dots in Figure 2a, show large variations of tidal ranges over the spring–neap cycle. The water-table data also revealed very strong spring-neap oscillations in all boreholes. In contrast, the semidiurnal and diurnal signals were much attenuated, except for borehole 1 (the most seaward one). Note that the water-table fluctuations shown in the figure have been scaled up by a factor of 10 (Figure 2c). The original water-table data are displayed in Figure 5. The plotted beach profile, along the center transect of the surveyed area, was measured on July 31 (Figure 2c). Apart from the cross-shore bars, the beach morphology is characterized by considerable along-shore variability (Figure 1a). The profiles changed during the entire field investigation period; in particular, differences between the profiles at the spring and neap tides were evident. However, such beach profile changes were not large enough to cause significant changes in the inland groundwater response to tides (LI, BAIRD, and HORN, unpublished data). For the purpose of simplicity and also because we focus on the beach behavior on July 31, we use the beach profile measured on that day in the simulation of tidal water-table fluctuations, ignoring the profile changes. Note that the elevations of the sea surface, beach surface, and groundwater table are all referenced to the ground level at borehole 1 where the origin of the coordinates is located.

The infrared camera was calibrated with a constant emissivity based on measured temperature data using a standard thermometer. The camera was connected to a personal computer (PC), which recorded the image every 15 minutes in a digital form (*i.e.,* a temperature matrix). The loggers of all the pressure transducers were synchronized with the PC.

DATA ANALYSIS, MODELING, AND DISCUSSION

Mapping of the Infrared Images

The raw image as shown in Figure 1b is mapped onto the physical plane based on the triangulation principle. For the purpose of simplicity, a two-dimensional transformation was adopted, *i.e.,* $(x, y) = \mathbf{F}(x_i, y_i)$, where x and y are the physical, horizontal coordinates (along- and cross-shore distances), and x_i and y_i are the image coordinates (row and column numbers in the temperature matrix). The transformation was based on four of the seven control points (CP): CPs 1, 4, 5, and 6; both their physical and image coordinates were used. The derived transformation was then verified using the information from CPs 2, 3, and 7. The transformation was used to determine the physical coordinates of each CP from its location on the image. The results shown in Figure 3 demonstrated that the mapped physical coordinates are very close to the surveyed coordinates, with errors of less than 2 m in distance.

Tidal Oscillations

For the tidal data, a harmonic analysis was conducted to recover the missing data at low tides when the sea level retreated seaward of the tidal transducer, using the following function:

$$h_{\text{tide}} = h_0 + \sum_{i=1}^{5} a_i \sin(\omega_i t + \delta_i). \quad (1)$$

The five tidal constituents included in the analysis are: S_2 ($\omega_1 = 0.5236$ rad h^{-1}), M_2 ($\omega_2 = 0.5059$ rad h^{-1}), N_2 ($\omega_3 = 0.4964$ rad h^{-1}), K_1 ($\omega_4 = 0.2625$ rad h^{-1}), and O_1 ($\omega_5 = 0.2434$ rad h^{-1}). A good fit of the data to the function was obtained with a high regression coefficient value, 0.95. The results show that the semidiurnal lunar tide (M_2) was the dominant signal (Table 1). These results were used to recover the missing tidal data that were required for the modeling (Figure 2).

Water-Table Fluctuations

The measured water-table fluctuations were analyzed to determine (1) the attenuation rates for particular frequencies, which give estimates of the transmissivity of the aquifer

This content downloaded from
152.15.113.8 on Thu, 14 Oct 2021 17:10:39 UTC
All use subject to https://about.jstor.org/terms

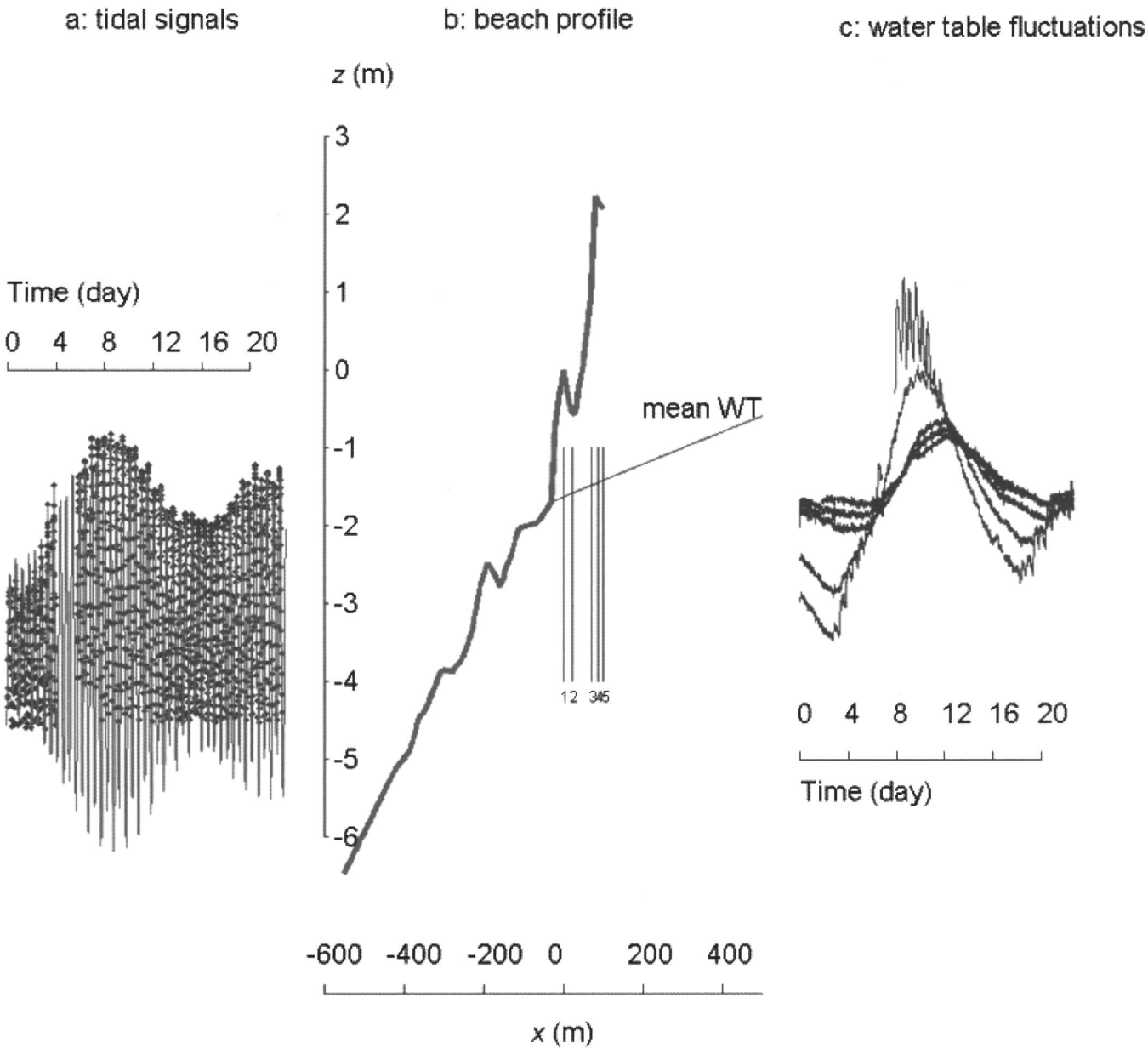

Figure 2. (a) Tidal signals, (b) beach profile along the central transect, and (c) observed water-table fluctuations in boreholes. The water-table fluctuations shown in the figure have been scaled up by a factor of 10.

and (2) the mean elevation of the water table. For these purposes, we fitted the water-table data for each borehole to a function similar to Equation (1) but with only two dominant spring–neap frequencies (ω_1–ω_2 and ω_2–ω_3). As mentioned previously, the diurnal and semidiurnal signals are attenuated much more rapidly. A good fit between the data and the function was obtained for all boreholes (with $r^2 \geq 0.92$). The fitted amplitude values are plotted in Figure 4. The exponential attenuation of the signals is evident and the damping rates were calculated: $\kappa = 0.0147$ m^{-1} for ω_1–ω_2 and 0.0127 m^{-1} for ω_2–ω_3.

Simple analytical solutions based on the linearized Boussinesq equation predict the following relationship between the damping rate and aquifer properties (hydraulic diffusivity, D) as well as the tidal frequency (ω) (*e.g.*, FERRIS, 1951):

$$\kappa = \sqrt{\frac{\omega}{2D}}, \tag{2}$$

where $D = T/S$ (T and S are the transmissivity and specific yield of the aquifer, respectively; $T = KH$, where K is the depth-averaged hydraulic conductivity and H the averaged

This content downloaded from
152.15.113.8 on Thu, 14 Oct 2021 17:10:39 UTC
All use subject to https://about.jstor.org/terms

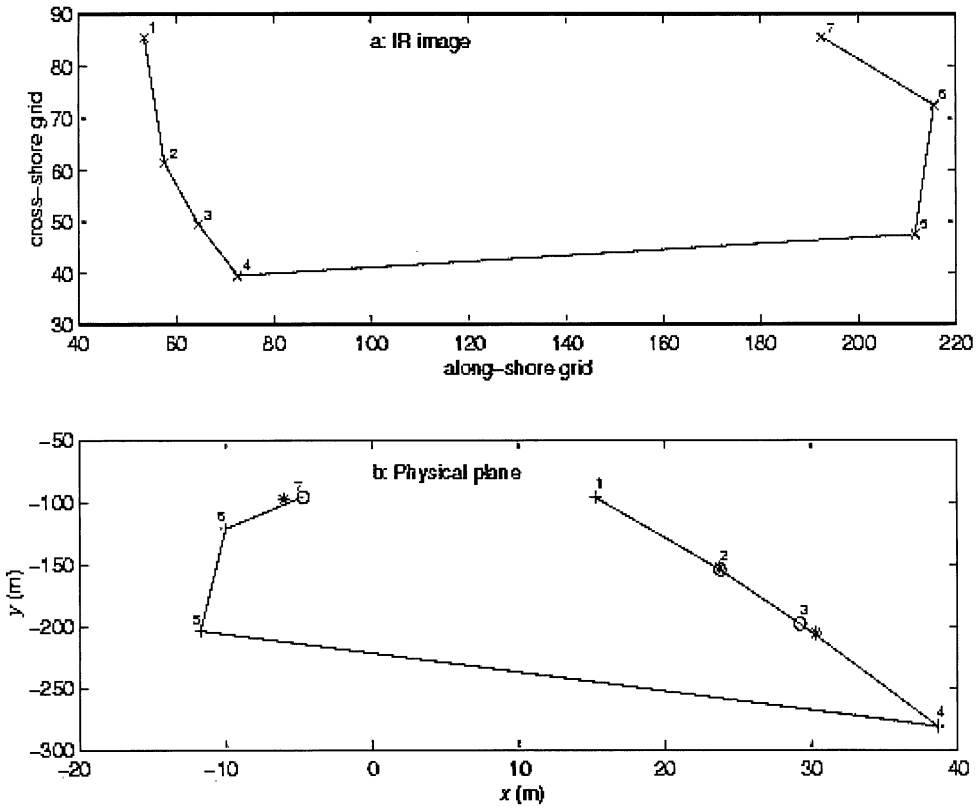

Figure 3. Mapping of the control points on the infrared image and the physical plane. Circles at CPs 2, 3, and 7 in (b) are determined by the derived transformation rule based on CPs 1, 4, 5, and 6. Note that the locations of these circles are close to those of the stars from surveying.

thickness of the aquifer). Based on the above estimates of κ and Equation (2), D was calculated in the range between 0.024 and 0.034 m²/s. The aquifer thickness H was determined from the borehole information to be around 23 m. Thus the value of K/S was estimated to be approximately 1.25×10^{-3} m/s. Three different values of K/S were used in the model simulations discussed below: 0.0006, 0.0011, and 0.0017 m/s. We estimated S around 0.2 based on the measured drainable porosity of the beach sands, giving an estimated value of K around 2.5×10^{-4} m/s. Slug tests were also conducted during the field experiment to measure the hydraulic conductivity. The K values determined from these tests ranged from 0.6×10^{-4} to 1.2×10^{-4} m/s. The slug test values are likely to be underestimates. The boreholes were not densely perforated. As a result, flow to the wells during the slug tests was likely retarded, giving too low a value of K when the Bouwer and Rice equation was used (Bouwer and Rice, 1976). Nevertheless, the estimates of K values based on the two different methods are reasonably close, giving confidence in the quality of data.

Table 1. *Results from the harmonic analysis of the tidal data.**

a_1	δ_1	a_2	δ_2	a_3	δ_3	a_4	δ_4	a_5	δ_5	h_0	r^2
0.49	2.47	1.62	5.82	0.40	1.94	0.18	5.64	0.15	4.04	−3.44	0.95

* a in meters and δ in radians.

The fitting of the water-table data to the function also gives the mean elevation of the water table at the boreholes' locations. Assuming a steady-state mean flow (averaged over the spring–neap cycle), the mean water table elsewhere can also be determined, especially at the landward boundary simulated in the model ($x = 500$ m).

Beach Groundwater Model—Governing Equation, Boundary Conditions, and Initial Conditions

The model is based on the two dimensional Boussinesq equation,

$$\frac{\partial h}{\partial t} = \frac{K}{S}\left[\frac{\partial}{\partial x}\left(h\frac{\partial h}{\partial x}\right) + \frac{\partial}{\partial y}\left(h\frac{\partial h}{\partial y}\right)\right], \quad (3)$$

where h is the height of the water table (*i.e.,* the water-table elevation with respect to the base of the aquifer, estimated to be located at $z = -25$ m at the field site). h is also a measure of the local hydraulic head in the aquifer. Equation (3) does not include the capillary effect, which has been previously thought to have little influence on the water-table fluctuation at the tidal (low) frequency (Li *et al.,* 1997). Recent studies demonstrated that as a result of hysteretic water retention, capillarity affects the water-table dynamics over a much wider range of frequencies, including the tidal frequency (Nielsen and Perrochet, 2000; Werner and Lockington, 2003). In the intertidal zone, the water table with trun-

This content downloaded from
152.15.113.8 on Thu, 14 Oct 2021 17:10:39 UTC
All use subject to https://about.jstor.org/terms

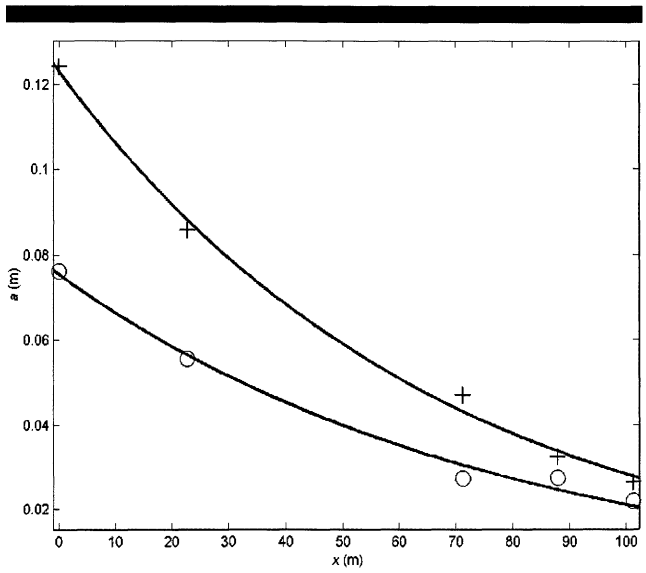

Figure 4. Amplitude damping of spring–neap oscillations in the boreholes (+ for ω_1–ω_2, ○ for ω_2–ω_3 and lines for fitted results). The solid lines are fitted curves of exponential decay to the data of ω_1–ω_2 and ω_2–ω_3, respectively.

cated capillary fringes can also be affected largely by capillarity (ATHERTON, BAIRD, and WIGGS, 2001). In both cases, the capillary effects lead to a significant reduction of the aquifer's specific yield. Physically, these effects result in much reduced fluctuations of the total moisture content in the beach sands in response to oscillations such as tides, while the beach water table may still experience large (> 10 cm) fluctuations. In the simulations presented here, we use the values of K/S estimated from the measured damping of tidal water-table fluctuations.

The simulation domain is as shown in Figure 2b (central, cross-shore section). The inland boundary is located at $x = 500$ m, where a zero gradient of h is specified. Other inland boundary conditions such as specified heads can also be applied. However, the water-table fluctuations in the nearshore area are likely to be insensitive to such boundary condition changes. The seaward boundary conditions are determined by the tides and the beach face elevations:

$$h(x, y, t) = Z(t) \quad \text{for } Z(t) > b(x, y), \tag{4a}$$

$$h(x, y, t + \Delta t) = b(x, y) \quad \text{if } h(x, y, t + \Delta t) > b(x, y) \text{ and } b(x, y) > Z(t), \tag{4b}$$

where $Z(t)$ is the tidal elevation (with respect to the base of the aquifer) and $b(x, y)$ is the elevation of the beach face from the beach survey carried out on July 31 (with respect to the base of the aquifer). Equation (4a) describes a tidal condition for the submerged beach area and (4b) expresses the condition of the seepage face where drainage takes place. These boundary conditions are essentially the same as those used in the GRIST model (BAIRD, MASON, and HORN, 1998). No special treatment is needed for the exit points of the water table at the beach face. Clearly, the grid points where the condition of Equation (4b) needs to be applied represent the seepage face and the exit point can be defined as the most landward or seaward node of these grid points. Note that because of the complex beach morphology (nonplanar beach profile), multiple, disconnected seepage faces were formed at the field site (LI, BAIRD, and HORN, 2002). The initial elevation of the water table seaward of borehole 5 was determined by interpolation between the measured, initial water-table elevations in boreholes 1 to 5. Landward of borehole 5, the water table was set at the mean elevation calculated as described above. A standard, explicit finite difference scheme was used to solve the governing equation. A small time step ($\Delta t = 0.5$ minutes) and grid size ($\Delta x = 2$ m and $\Delta y = 2$ m) were used in the simulations discussed below to ensure the numerical stability and accuracy of the results. The simulations started from day 1, July 15, and ran for the entire field trip period (*i.e.,* until August 4).

Simulated Tidal Water-Table Fluctuations in the Boreholes

Simulations were conducted with three different values of K/S. These values were selected based on the estimates from the above amplitude damping analysis. The results allow us to assess the sensitivity of the predicted water-table behavior to the hydraulic properties of the aquifer. The predictions from the second simulation (with $K/S = 0.0011$ m/s) agree reasonably well with the data (Figure 5a). In particular, both short period (semidiurnal and diurnal) and long period (spring–neap) water-table fluctuations that occurred in boreholes 1 and 2 were reproduced in the simulations. Although the semidiurnal signals were overpredicted, the essential features of these oscillations—the asymmetry between the rising and falling water tables, and the occurrence and phase of each semidiurnal water-table peak in response to semidiurnal high tides—were captured by the model simulations. The magnitude and phase of the spring and neap water-table fluctuations were also predicted. The main deficiency is the underprediction of the mean water-table elevations in all the boreholes. The cause of this may partly be the applied initial conditions of the water tables, especially for areas outside the measurement zone. Because of the lack of data, the mean water-table elevations calculated from the data-fitting function were used as the initial water-table elevations for these areas. Prior to the field deployment, there were several rainfall events, which could have led to a recharge of the aquifer and an increase in water-table levels. This recharge was not considered in the model simulations.

The first and third simulations gave less satisfactory results (Figures 5b and c). The sensitive response of the model predictions to the change of the K/S values reflects the dependence of the water-table behavior on the aquifer's hydraulic properties.

The reasonable agreement between the predicted and observed borehole water-table fluctuations provides confidence in the model. In the following section, we use the model to investigate the change of the water-table depth in the intertidal zone. The analysis, focusing on the falling tide period on July 31, examines the possible relationship between the

This content downloaded from
152.15.113.8 on Thu, 14 Oct 2021 17:10:39 UTC
All use subject to https://about.jstor.org/terms

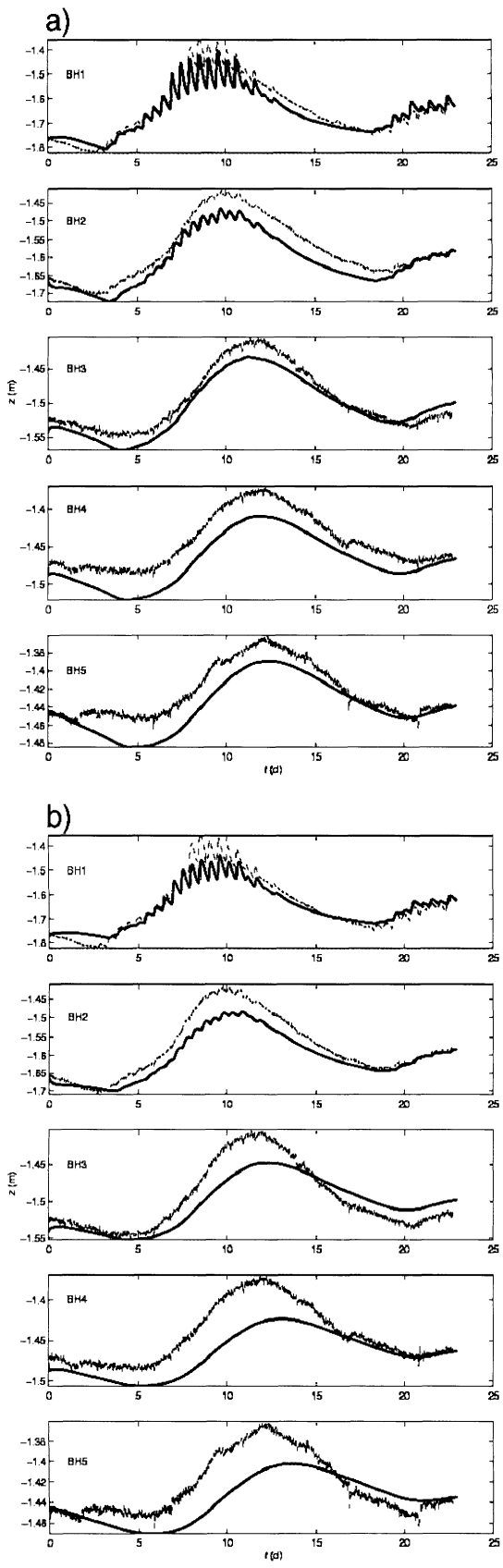

Figure 5. Comparison between measured and simulated water-table fluctuations in boreholes: (a) $K/S = 0.0011$ m/s; (b) $K/S = 0.0006$ m/s; and (c) $K/S = 0.0017$ m/s. Dotted line is for measurement and solid line for predictions.

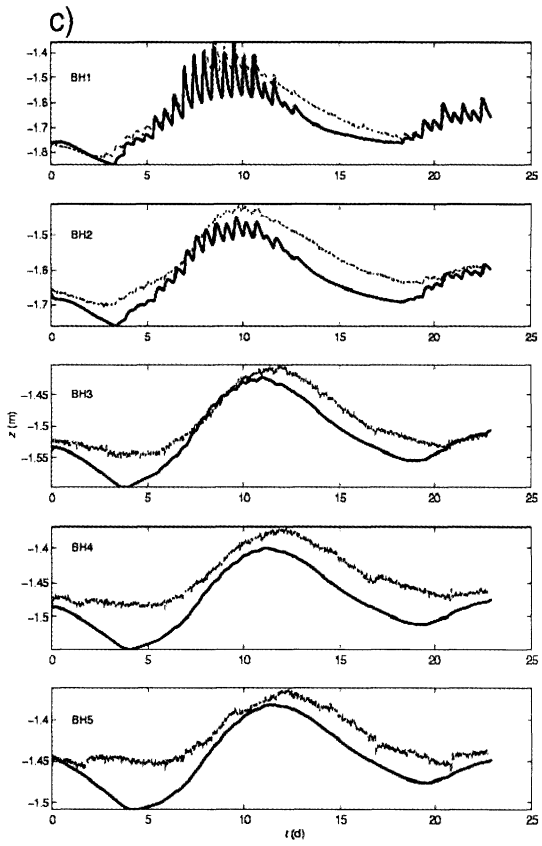

Figure 5. Continued.

water-table depth and surface temperature in the intertidal zone.

Dynamics of the Intertidal Zone—Depth of the Water Table and Beach Surface Temperature

Previous studies have shown that the beach surface temperature varied by several degrees when it was exposed during the falling tide. Our infrared data also indicated considerable increase in surface temperature as the tide receded. The temperature changes were, however, nonuniform. In Figures 6b and 7b, we plot the spatial temperature variations (temperature color image superimposed on the beach surface) at two different times: when the tide started to recede and when it almost reached low tide. The temperature variations seem to be related to the beach morphology. The locations of high and low temperatures appear to correspond to relatively high and low bed elevations in the beach profile. In particular, the temperature tended to be relatively high at the top of the berms and bars. While the heat source was the solar radiation, the bed elevation differences were not large enough to directly cause the temperature variations. On the other hand, the beach morphology affects the drainage characteristics of the beach face and hence the beach water-table depth. Based on the simulated beach water-table elevations, the water-table depths were calculated by subtracting the simulated water-table elevation from the bed elevation. The

This content downloaded from
152.15.113.8 on Thu, 14 Oct 2021 17:10:39 UTC
All use subject to https://about.jstor.org/terms

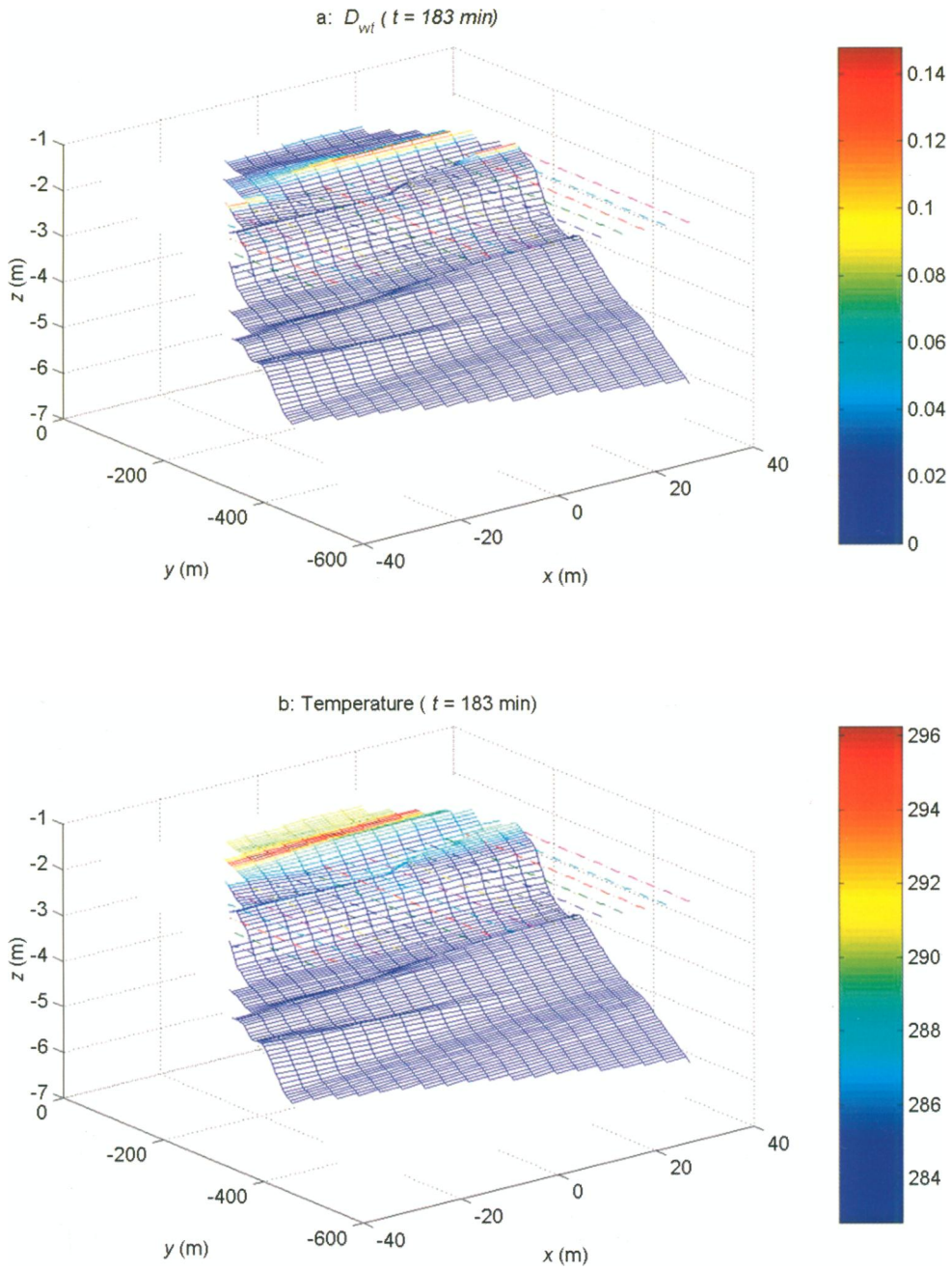

Figure 6. Comparison between the spatial variations of beach surface temperature and water-table depth at t = 183 min. The straight lines indicate the tidal sea levels. The color bars indicate the (a) water table depth in meters and (b) surface temperature in degrees Kelvin.

spatial variations of the water-table depths exhibited similar patterns to those of the temperatures (Figures 6a and 7a). To explain such similarity, we hypothesize a heating mechanism based on the depth of the simulated water table in the intertidal zone. The assumption is that the temperature is controlled by the local heat capacity of the exposed sand surface, which decreases with the water-table depth. Furthermore, the thermal conductivity will decrease as the beach dries, resulting in a reduction of the heat flux (heat loss) into the sand. Therefore, a large water-table depth is expected to lead to a high temperature of the beach surface exposed to solar radiation (heat source).

To examine further the relationship between the water-table depth and surface temperature, we compared the temporal variations of these two parameters along the central transect on the falling tide (Figure 8). With respect to the

This content downloaded from
152.15.113.8 on Thu, 14 Oct 2021 17:10:39 UTC
All use subject to https://about.jstor.org/terms

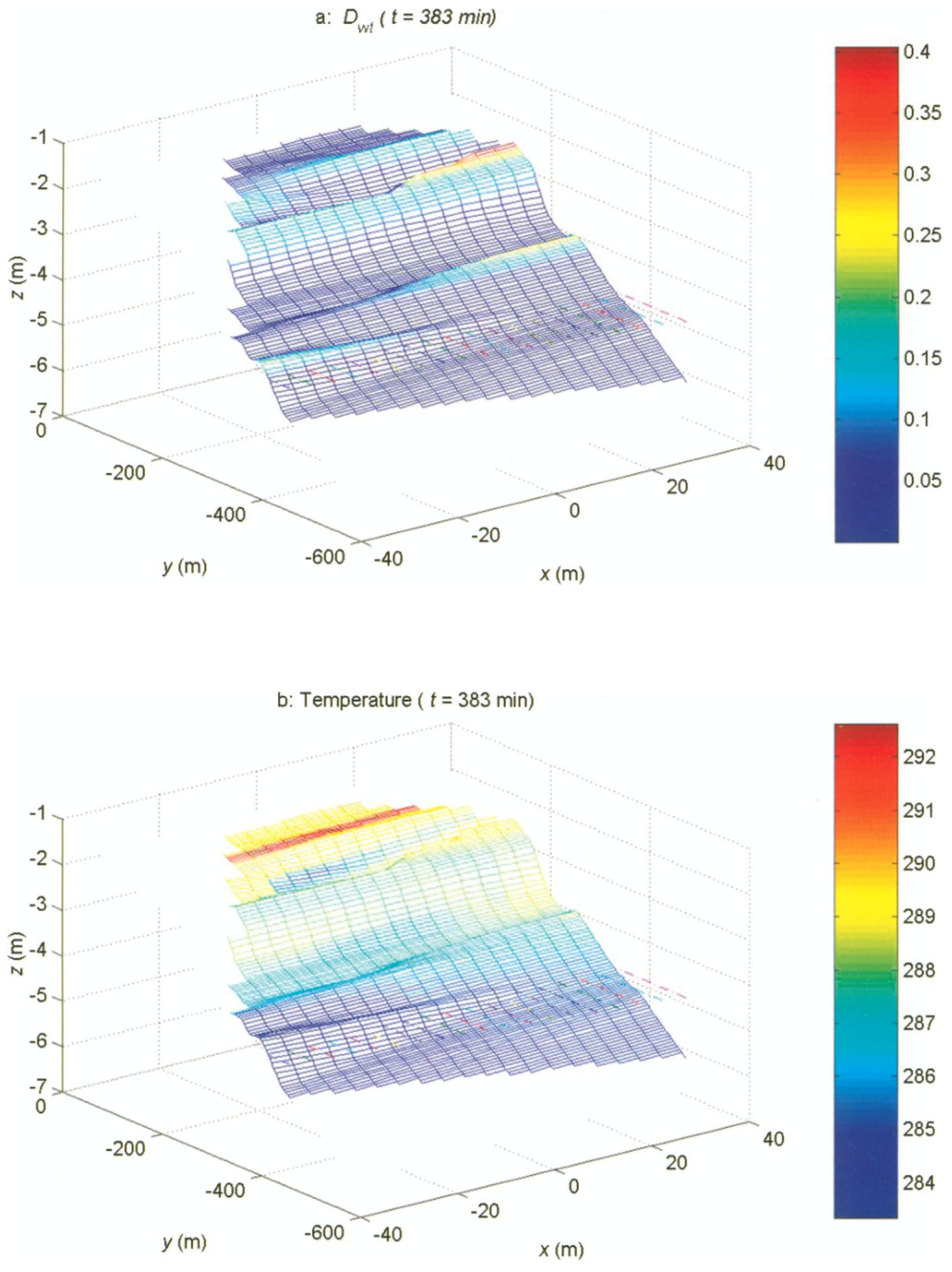

Figure 7. Comparison between the spatial variations of beach surface temperature and water-table depth at $t = 383$ min. The straight lines indicate the tidal sea levels. The color bars indicate the (a) water table depth in meters and (b) surface temperature in degrees Kelvin.

first parameter, five bands of deep and shallow water-table areas are evident (lower panel). The formation of these bands was obviously due to the local beach morphology that affected the water drainage from the beach as the tide receded. The temperature changes are characterized by an overall increase as the tide receded. The increase in temperature reached constant levels rather quickly. The second feature of the temperature profile is the band structure of alternating high and low temperatures. Near the landward berm area (around $y = -100$ m), the two temperature bands (I, high and II, low) correspond with the two water-table bands (I, deep and II, shallow). Such correspondence is however not evident in the two seaward bar areas ($y = -200$ and -300 m). While the water-table bands are still distinct in these two areas, the temperature profile exhibits no such feature, suggesting that the heat transfer process is much more complicated than de-

This content downloaded from
152.15.113.8 on Thu, 14 Oct 2021 17:10:39 UTC
All use subject to https://about.jstor.org/terms

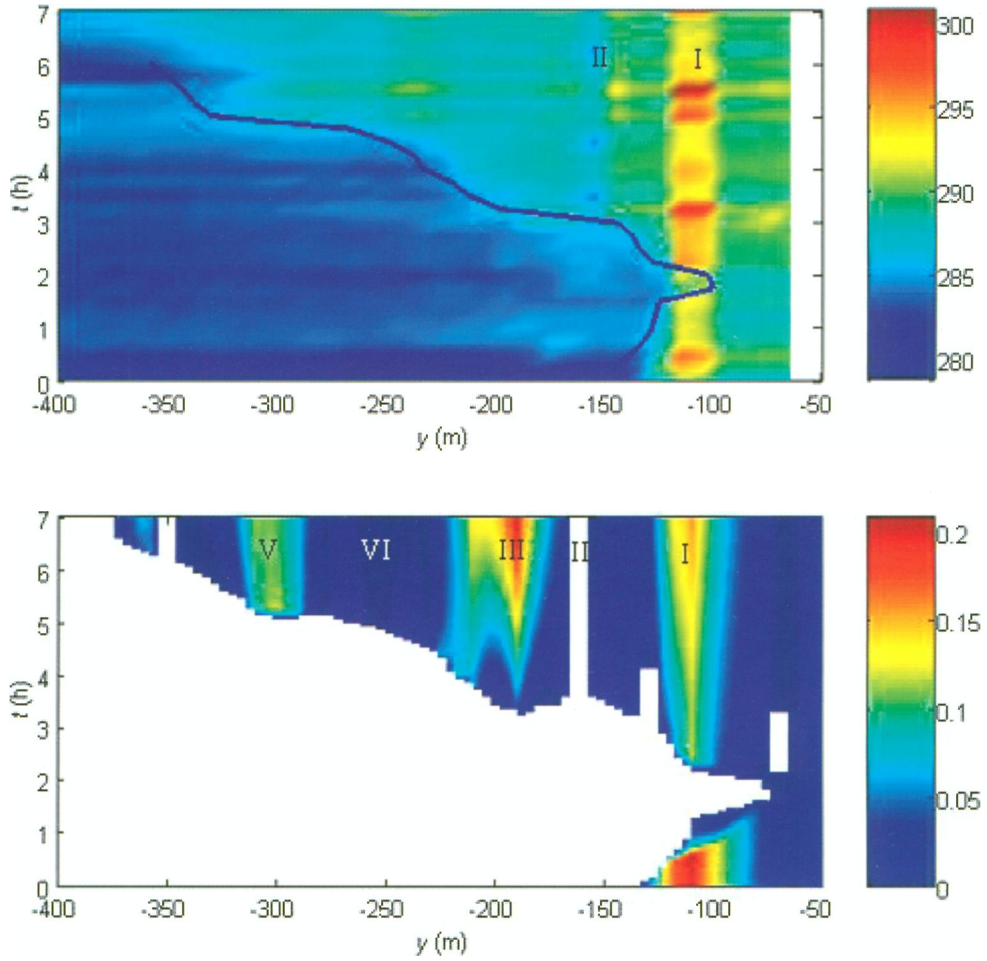

Figure 8. Temperature changes (upper panel) and water-table depth variations (lower panel) along the central transect.

scribed by the simple mechanism investigated here. Relatively short exposure time for the seaward bar area compared with that for the landward berm area might have limited the heating of the former area. The exposure-time effects were, however, complicated as shown in the behavior of the surface temperature on the landward berm, which did not increase monotonically with the exposure time. Other factors such as winds and changes of sunlight intensity due to clouds also influenced the surface temperature, possibly smearing the differences between the bands. Moreover, the heat capacity of beach sands depends on the local water content rather than being simply related to the water-table depth. ATHERTON, BAIRD, and WIGGS (2001) showed that the local water content, unlike the water table, is much less responsive to tidal oscillations. To account fully for these factors and processes, we would require a more comprehensive model that incorporated heat exchange between the sand surface and the ambient air, and the heat loss to the beach groundwater including water in the unsaturated zone (*e.g.,* HYDROTHERM; HAYBA and INGEBRITSEN, 1994). Notwithstanding these complexities, the results suggest that the beach water-table depth and surface temperature are interrelated parameters, both affected by the tides.

In the previous section, we have examined only the variations of beach conditions induced by semidiurnal (half-day period) tides. In reality, oscillations occur over a much wider range of frequencies; for example, seasons and the spring–neap cycle (of 14.78 days). At the field site, the observations showed significant water-table responses to the spring–neap fluctuations of the tidal range in all the boreholes. The numerical simulations revealed considerable differences between the averaged water-table depths during spring and neap tides (Figure 9). The beach water table is deeper during the neap tide than during the spring tide. This suggests that the beach surface may tend to be warmer during the neap tide than during the spring tide given similar conditions of surface heating (weather conditions).

The spring–neap variations of the water-table depth in the intertidal zone are further evident in Figure 10, where the comparison between two morphologically different locations is made. The two locations are both on the central transect, one at a ridge and the other at a runnel (shown on the top

This content downloaded from
152.15.113.8 on Thu, 14 Oct 2021 17:10:39 UTC
All use subject to https://about.jstor.org/terms

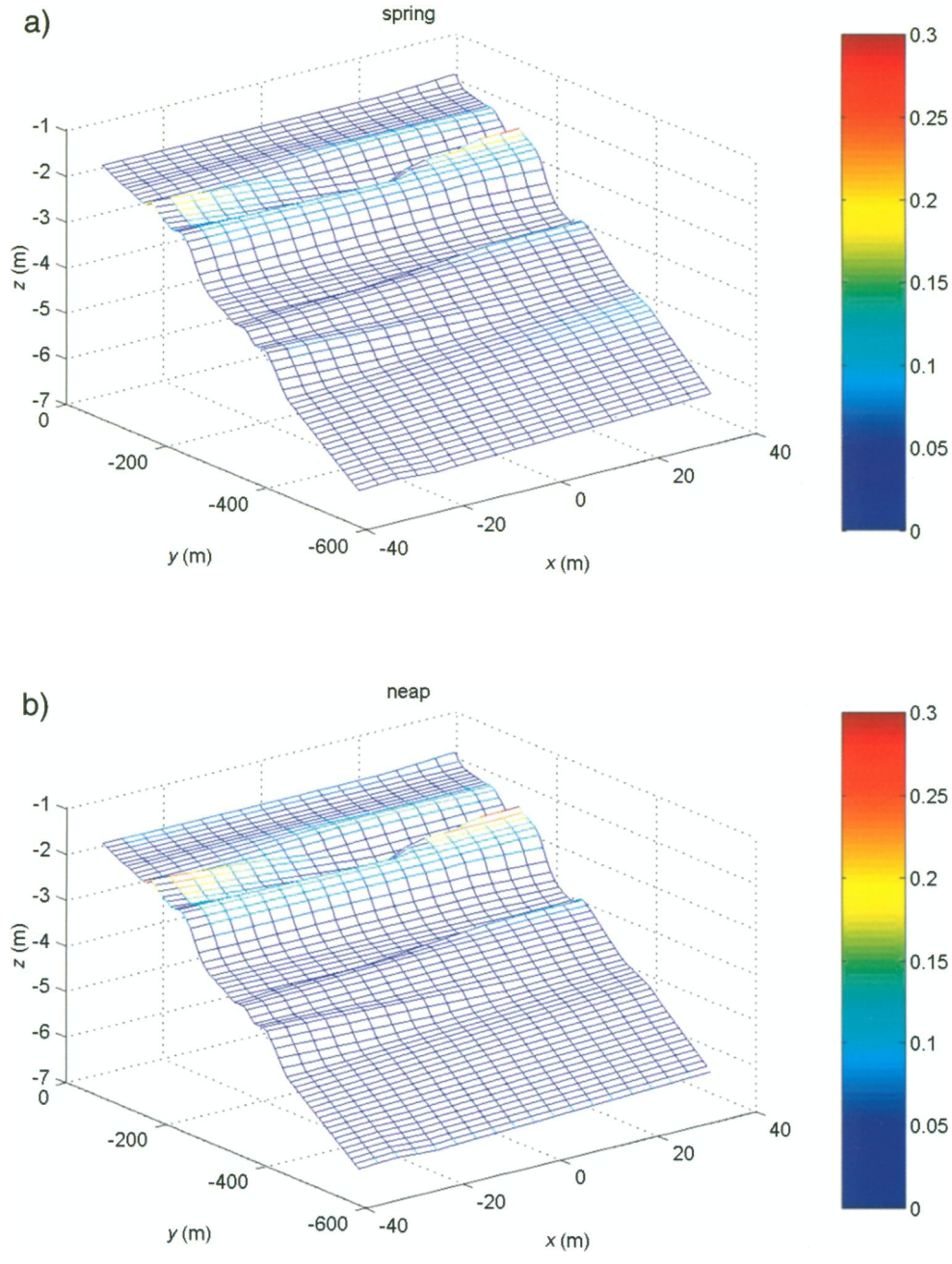

Figure 9. Averaged water-table depth during (a) spring and (b) neap tides.

panel of the figure). Again the water-table depth was calculated by subtracting the simulated local water-table elevation from the bed elevation. When the beach was submerged, the water-table depth became undefined. Each segment of the discontinuous curves of the water-table depth represented the drainage phase of the exposed beach as the tide receded. The water-table depth increased until the rising tide reached the locations. The beach was submerged between two adjacent segments. At both locations, the water-table depth was larger during the neap tides than that on the spring tides. However, the water table was nearer the beach surface at the runnel than at the ridge, implying that the beach could be drier at the latter location. Moreover, the water table fell faster at the ridge as the tide receded (*i.e.,* the water-table depth increased more rapidly). These results demonstrate the effects of local beach morphology on the beach conditions in the intertidal zone, especially the water-table depth and the associated moisture content and temperature.

This content downloaded from
152.15.113.8 on Thu, 14 Oct 2021 17:10:39 UTC
All use subject to https://about.jstor.org/terms

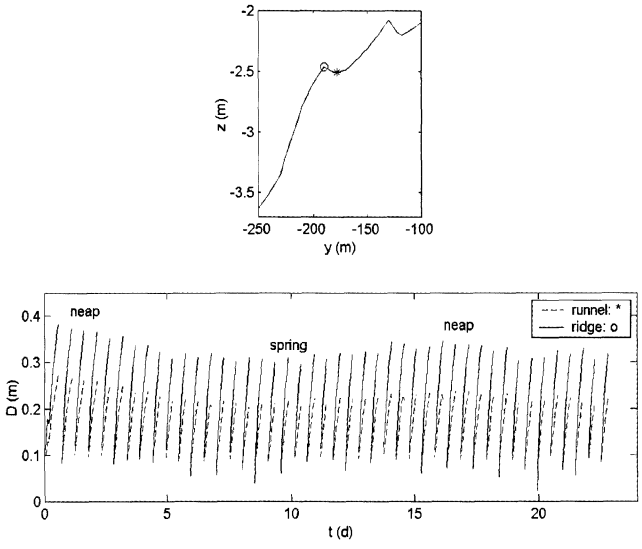

Figure 10. Comparison of the water-table depth at a ridge and a runnel (locations shown on the top panel) on the beach.

CONCLUDING REMARKS

Water-table depth and temperature are important parameters of the beach condition for interstitial fauna. In the intertidal zone, both parameters are largely influenced by the tide. The experimental study presented here shows that:

- The behaviors of the beach water-table depth and temperature during the falling tide are considerably affected by the beach morphology. Beach berms and bars are relatively dry and can become warmer than the adjacent low area.
- The beach water-table depth and temperature are interrelated parameters; in particular, the former modifies the response of the latter to the solar radiation (as the heating source).
- The beach environment is much more complex than described in the groundwater flow and surface heating models presented. The water-table depth is not always a good indicator or measure of the beach water content. To simulate the water content changes, we need to consider the capillary effects. For the temperature variations, a full heat transfer model considering the heat exchange between the beach and the ambient air would be required.

ACKNOWLEDGMENT

This work is funded by Natural Environment Research Council, UK, under research grant NER/B/S/2000/00770.

Comments from two anonymous reviewers have led to improvement of the paper and are greatly appreciated.

LITERATURE CITED

ATHERTON, R.J.; BAIRD, A.J., and WIGGS, G.F.S., 2001. Inter-tidal dynamics of surface moisture content on a meso-tidal beach. *Journal of Coastal Research,* 17, 482–489.

BAIRD, A.J., and HORN, D.P., 1996. Monitoring and modelling groundwater behaviour in sandy beaches. *Journal of Coastal Research,* 12, 630–640.

BAIRD, A.J.; MASON, T., and HORN, D.P., 1998. Validation of a Boussinesq model of beach groundwater behaviour. *Marine Geology,* 148, 55–69.

BOUWER, H. and RICE, R.C., 1976. Slug test for determining hydraulic conductivity of unconfined aquifers with completely or partially penetrating wells. *Water Resources Research,* 12, 423–428.

CAMPBELL, E.E., and BATE, G.C., 1998. Tide-induced pulsing of nutrient discharge from an unconfined aquifer into an Anaulus Australis-dominated surf-zone. *Water SA,* 24, 365–370.

CARTWRIGHT, N.; NIELSEN, P., and LI, L., 2004. Experimental observations of watertable waves in an unconfined aquifer with a sloping boundary, 1. Sand flume experiments. *Advances in Water Resources,* 27, 991–1004.

FERRIS, J.G., 1951. Cyclic fluctuations of water level as a basis for determining aquifer transmissibility, *IAHS Publication,* 33, 148–155.

HAYBA, D.O., and INGEBRITSEN, S.E., 1994. The computer model HYDROTHERM, a three-dimensional finite-difference model to simulate ground-water flow and heat transport in the temperature range of 0 to 1,200 degrees Celsius. *US Geological Survey Water-Resources Investigations Report* 94-4045, 85 pp.

LI, L.; BAIRD, A.J., and HORN, D., 2002. Spring-neap tidal water table fluctuations in a coastal aquifer: beach slope vs seepage face effects. *Proceedings of the 28th International Conference on Coastal Engineering* (New York, World Scientific), pp. 1037–1049.

LI, L.; BARRY, D.A.; PARLANGE, J.Y., and PATTIARATCHI, C.B., 1997. Beach water table fluctuations due to wave runup: Capillarity effects. *Water Resources Research,* 33, 935–945.

LI, L.; BARRY, D.A.; STAGNITTI, F.; PARLANGE, J.-Y., and JENG, D.S., 2000. Beach water table fluctuations due to spring-neap tides: moving boundary effects. *Advances in Water Resources,* 23, 817–824.

MCINTYRE, A.D., 1969. Ecology of meiobenthos. *Biological Reviews of the Cambridge Philosophical Society,* 44, 245–290.

NIELSEN, P., 1990. Tidal dynamics of the water table in beaches. *Water Resources Research,* 26, 2127–2134.

NIELSEN, P. and PERROCHET, P., 2000. Watertable dynamics under capillary fringes: experiments and modelling. *Advances in Water Resources,* 23, 503–515.

POLLOCK, L.W. and HUMMON, W.D., 1971. Cyclic changes in interstitial water content, atmospheric exposure, and temperature in a marine beach. *Limnology and Oceanography,* 16, 522–535.

RAUBENHEIMER, B.; GUZA, R.T., and ELGAR, S., 1999. Tidal water table fluctuations in a sandy beaches. *Water Resources Research,* 35, 2313–2320.

STIMSON, A., 1974. *Photometry and Radiometry for Engineers.* New York: Wiley, 446 pp.

TURNER, I., 1993. Water table outcropping on macro-tidal beaches: A simulation model. *Marine Geology,* 115, 227–238.

WERNER, A. and LOCKINGTON, D.A., 2003. Influence of hysteresis on tidal capillary fringe dynamics in a well-sorted sand. *Advances in Water Resources,* 26, 1199–1204.

This content downloaded from
152.15.113.8 on Thu, 14 Oct 2021 17:10:39 UTC
All use subject to https://about.jstor.org/terms